Short title: **ROS modulates lignin & silica deposits**

Corresponding author: Rivka Elbaum, rivka.elbaum@mail.huji.ac.il

Full title: **Hydrogen peroxide modulates lignin and silica deposits in sorghum roots**

Nerya Zexer and Rivka Elbaum*

The Robert H. Smith Institute of Plant Sciences and Genetics in Agriculture, The Hebrew University of Jerusalem, 7610001 Rehovot, Israel

One sentence summary: Lignin with carbonyl modifications is patterned by the activity of H_2O_2 and peroxidases to nucleate silica aggregations in sorghum roots.

Author Contribution

Both authors conceived and designed the experiments. N.Z conducted the experiments, and both authors analyzed the data and wrote the manuscript.

The research was funded by the Israeli Ministry of Agriculture & Rural Development, Chief Scientist Office grant 12-01-0016. N.Z is thankful to the Robert H. Smith Foundation for a scholarship.

* Corresponding author: rivka.elbaum@mail.huji.ac.il, +972-8-9489335

Abstract

Silica aggregates in the root endodermis of grasses. Availability of Si to roots is associated with variations in the balance of reactive oxygen species (ROS) and increased resistance to drought, *Striga*, salt and heavy metals. In sorghum (*Sorghum bicolor* L.), silica aggregation is patterned in an active silicification zone (ASZ) by a special type of lignin. Since lignin polymerization is mediated by ROS, we studied the formation of root lignin and silica under varied conditions of ROS and specifically hydrogen peroxide (H_2O_2). Sorghum seedlings were grown hydroponically under varied Si and oxidative levels. Lignin and silica deposits in the endodermis were studied by optical, scanning electron, and Raman microscopies. Cell wall composition was quantified by thermal gravimetric analysis. Silica aggregation was catalyzed by lignin modified by carbonyls. These residues were available for silica nucleation only within 2 hours of their deposition. The endodermal H_2O_2 concentration regulated the intensity but not the pattern of ASZ lignin deposits. Our results imply that localized secretion of modified monolignols is necessary for patterning ASZ lignin. Fast silica aggregation may locally inhibit lignin polymerization and transiently increase H_2O_2 levels. Such momentary local high ROS concentrations may convey Si-induced stress tolerance in the root.

Key words: Active silicification zone; Endodermis ITCW; Hydrogen peroxide; Lignin; Silica aggregates; Silicic acid

Introduction

Silicone oxides are the most abundant mineral group in soils. Therefore, plant roots are always exposed to some silicic acid ($Si(OH)_4$), which is the soluble form of silicates. Rice, barley, cucumber and tomato, among other plants, express silicon transporters in their roots (Mitani-Ueno and Ma, 2020). Concerted expression causes super saturation of silicic acid in the xylem sap (Sakurai et al., 2015) in wheat, rice, sorghum and other grasses (Casey et al., 2004; Mitani et al., 2005; Soukup et al., 2019). The silicic acid is transported to the shoot by the transpiration stream, and deposited as biogenic opaline silica ($SiO_2 \cdot nH_2O$). This may lead to accumulation of up to 10% silica per tissue dry weight. The deposition may take various mechanisms that are mostly unknown (Hodson, 2016). Heavily silicified locations may be adjacent to cells that are not silicified at all (Lawton, 1980; Bennett, 1982), suggesting a biologically-controlled process. Silica may also form in roots and leaves starved for silicic acid (Kumar et al., 2017; Zexer and Elbaum, 2020), suggesting that the biological entities concentrate residual silicic acid to saturation level at silicification loci. Dissolution of silica bodies from the grass *Phalaris canariensis* and the fern *Equisetum telmatenia* by hydrofluoric acid releases protein residues made of a large fraction of acidic amino acids and basic lysine, which may regulate nucleation of the silica (Harrison, 1996). Dissolving silica bodies from wheat in ammonium fluoride released degraded oligo-proteoglycans (Elbaum et al., 2009). Lipids are also detected in plant silica (Smith and Anderson, 2001; Zancajo et al., 2019), possibly originating from cuticle waxes trapped inside the mineral (Yoshida, 1981). Recently, we reported the first protein that causes silica formation in plants. Siliplant1 (Slp1) is expressed in sorghum (*Sorghum bicolor* L.) epidermis cells called silica cells. It is exported to the cell wall, where it interacts with supersaturated silicic acid solution. Slp1 catalyzes the formation of a thick silica wall within hours (Kumar et al., 2020). In parallel, the cell cytoplasm shrinks into threads, and eventually evacuated during a programmed cell death (Kumar and Elbaum, 2018).

Silica is also found in sorghum roots, at very specific locations in the cell walls of the endodermis (Sangster and Parry, 1976; Lux et al., 2003; Soukup et al., 2017). However, no Slp1 is expressed in this tissue (Kumar et al., 2020). In contrast to leaves, root silica forms on densely deposited lignin with peculiar characteristics. At about 4-8 cm from the root tip, we define an active silicification zone (ASZ). In this region, specialized ASZ lignin forms a spotted pattern that nucleates silica aggregation (Figure 1). These lignified locations polymerize residual amounts of silicic acid (Zexer and Elbaum, 2020), suggesting that the deposits play an important, yet unknown biological function. Lignin is a polyphenol polymer constructed from monolignols at the cell wall. Monolignols are synthesized in the cytosol from phenylalanine and transported to the apoplast, where their polymerization is catalyzed by

69 the activity of peroxidases and laccases. Plant Peroxidases are iron containing enzymes that use H_2O_2
70 to radicalize monolignols. Laccases are glycoproteins that oxidize monolignols using a copper
71 containing oxidation center. The activity of both enzymes results in monolignol radicals free to react
72 with the growing lignin polymer (Wang et al., 2013; Meents et al., 2018). Several models aiming to
73 explain cellular export of monolignol have been hypothesized. Namely, by vesicle-mediated
74 exocytosis, via activity of membrane localized transporters, and passive diffusion through the cell
75 membrane. However, while lignification is undoubtedly a tightly regulated process in both space and
76 time, there is currently no clear evidence for the directed secretion of lignin building blocks (Meents et
77 al., 2018). Formation of local deposits of lignin is achieved by the localized binding of laccases and
78 peroxidases complexes to the cell wall (Lee et al., 2013; Schuetz et al., 2014; Hoffmann et al., 2020).
79 Endodermal lignification is enhanced under silicic acid treatments and appears in younger root tissues
80 treated with silicic acid, as compared to roots starved for silicic acid (Fleck et al., 2011; Lukačová et
81 al., 2013). This may suggest that in addition to general lignin, ASZ lignin may also appear earlier under
82 silicic acid treatment. Therefore, in this work we explored the effect of ROS variation on lignin and
83 silica formation in roots of sorghum seedling. Our results indicate a local secretion of ASZ lignin
84 monomers that react with H_2O_2. The freshly polymerized ASZ lignin nucleates silicic acid into silica.
85
86

Results

To study the reciprocal influence of silicic acid and H_2O_2 we mapped ROS along roots grown with (Si+) and without (Si-) silicic acid by staining with 3,3′-Diaminobenzidine (DAB) (Figure 2). DAB is oxidized in the presence of H_2O_2 and heme-containing enzymes. As a result, dark precipitates form in stained tissues (Daudi and O'Brien, 2012). Since laccases lack the ability to oxidize DAB, this staining method can be viewed as an indicator for peroxidases activity (Barceló, 1995). Brown staining was identified in region II, where silica aggregation is initiated (Figure 1). A continuum of brown discoloration formed from the endodermal inner tangential cell wall (ITCW) to the nearest metaxylem element. The staining along the roots was similar between Si- and Si+ treatments (Figure 2a-f). Nonetheless, under Si- treatment the ITCW innermost layer in region III revealed a pattern of darker DAB-stained spots (Figure 2g). In the same region under Si+ treatment, we detected dark rings on a uniformly DAB-stained background ITCW (Figure 2h). Both spots and ring, which indicated high peroxidase and ROS activity, formed a pattern similar to that of silica aggregation. This suggests that activity of ROS varies in relation to the formation of the root silica aggregates.

Root ROS levels positively correlate to silica aggregate footprint

In order to examine the influence of ROS levels on the aggregation of silica we aimed to increase the production of endogenous ROS at the endodermis. For this, we poked roots of Si- seedlings by a syringe needle. Immediately after the injury, the plants were transferred to Si+ hydroponic media for recovery. After 3 days, no aggregates formed at the injury location, possibly due to tissue damage and cell death. Adjacent to the injury, the average footprint of the silica aggregates on the ITCW was larger in relation to aggregates that developed in parallel regions of uninjured roots (Figure 3). This supports the hypothesis that ROS produced during injury may enhance silica deposition.

Increased ROS may be produced also in salt-stressed roots. We thus subjected roots to a salinity stress by transferring Si- seedlings to Si+ hydroponics media supplemented with 50 mM NaCl. In these roots, too, we found larger silica aggregates compared to non-stressed roots (Figure 4). Direct addition of H_2O_2 to the hydroponics solution also increased the average footprint of the silica aggregates (Figure 4). Interestingly, the increase in projected area was negatively correlated to the H_2O_2 concentration. We therefore continued to explore the influence of small variations in the oxidative balance on silica aggregation.

Initiation of lignin and silica patterns are influenced similarly by ROS balance

The effect of H_2O_2 on the development of the young tissue at the root tip was analyzed separately from the deposition of lignin in the mature parts of the root (region I vs. II-III, Figure 1). For this, seedlings

were grown for 3 days in Si- hydroponics solution, allowing a mature lignified but not silicified tissue to develop. On the 4th day, the seedlings were transferred to Si+ hydroponics solution supplemented with 0.5 mM H_2O_2 for additional 3 days. This allowed a younger part of the root to develop under oxidative stress and silicic acid. In another treatment, 1 mM KI was added, which quenched physiological H_2O_2, reducing the native ROS concentration. We then tested these roots for silica aggregate formation in three regions: (1) young developing tissue about 1 cm from the root tip, developing under altered ROS balance (region I), (2) mature region composed of cells that were exposed to silicic acid in parallel to completing their maturation under high/low ROS concentrations (region III), and (3) mature region, containing cells that were exposed to silicic acid only after completing their development under benign conditions (region IV). H_2O_2 treatment considerably stunted root growth, while under KI treatment the average length of the roots was similar to that of untreated samples (Figure 5a-c). In the mature part of the roots (region IV), the silica deposition was similar between all treatments (Figure 5d-f). However, silica aggregation was detected already in region I under H_2O_2, and only in region IV under KI (Figure 5f-l). Our results suggest that developmental processes in the young root that respond to the altered ROS levels affect silica aggregation. Such a process may presumably be lignin deposition.

In order to follow the formation of the lignin spots in the endodermis, 6 days old roots grown under Si+ and Si- treatments were stained for lignin by phloroglucinol-HCl (Figure 6). In the Si+ roots, the ITCW exhibited spots of staining intensity lower than the staining of the background ITCW, possibly indicating silica aggregation. In the Si- treatment, spots of increased staining were pattered similarly (Figure 6a-f). We then examined 6-days old Si- roots that were grown for 3 days under H_2O_2 or KI treatments. The phloroglucinol-HCl staining behaved similarly to the silica aggregation pattern revealed in Figure 5: Under H_2O_2 treatment spots initiated in region I, and under KI treatment spots were found only in region IV (Figure 6g-l). Quantitative comparison of the patterns of Si+ and Si- roots was achieved by autofluorescence microscopy, showing silica aggregation in blue (Soukup et al., 2014) and ASZ lignin in green (Zexer and Elbaum, 2020). The distance from the root tip to the first blue (Si+) or green (Si-) spot was measured under H_2O_2 or KI treatments (Figure 7). Under all ROS regimes, the average distance to the first fluorescent spot was similar between Si+ and Si- treatment. We therefore concluded that the aggregates in Si+ and the lignin spots in Si- roots represent the same oxidative phenomenon in the same locations and developmental stage.

Lignin spotted pattern is depressed by KI

To test whether the lignin spots are a prerequisite for the aggregation of silica we first quantified the disturbance in lignin formation under KI treatment in Si- roots. Thermal gravimetric analysis revealed four decomposition peaks, assigned to lignin, cellulose, and hemicellulose (Figure 8) (Yang et al., 2007). The lignin decomposition temperature was similar between the samples, at 434 ± 44ºC. The cellulose decomposed in two stages, at 311 ± 3ºC and 323 ± 2ºC, similarly in both treated and non-treated samples. However, in KI treated roots the hemicellulose decomposed at a lower temperature (266.5 ± 0.3ºC) than the non-treated roots (283 ± 4ºC). We detected no statistically significant variation in the fractions of these three main components of the cell wall (Figure 8).

Raman micro-spectroscopy was used to monitor lignin composition and distribution (Figure 9). Average spectra of whole Raman maps showed typical lignocellulosic trace, with major cellulose peaks at 378, 1095 cm^{-1}, and lignin at 1171, 1600, 1630, 1660 cm^{-1} (Agarwal and Ralph, 1997; Agarwal, 2014). The KI treated sample average spectrum showed smaller scatterings of lignin at 1171, 1200 cm^{-1} than the control spectrum (Figure 9a). Spectral first derivative enhanced hidden peaks and reduced fluorescence background. Derivation of the aromatics doublet at 1600-1630 cm^{-1} revealed peak shoulders at 1585 and 1660 cm^{-1} only in the non-treated control roots (Figure 9b,c). The 1585 cm^{-1} shoulder was assigned to lignin in sugarcane (Agarwal, 2014), and the 1660 cm^{-1} to lignin in black spruce (Agarwal and Ralph, 1997). Mapping the total Raman signal in non-treated roots revealed a spotted pattern, suggesting that the cell wall in these locations is denser than their surroundings (Figure 9d). This is in accordance with our published finding of higher intensity of SEM back scattered electrons at the spots, relative to the surrounding cell wall (Zexer and Elbaum, 2020). In the KI treated samples no spots were identified, suggesting that dense cell wall did not develop (Figure 9e).

In order to identify specific Raman peaks related to the spots while compensating for the general higher signal, we mapped lignin peaks normalized to the crystalline cellulose peak at 378 cm^{-1} (Figure 9f-k). Interestingly, the aromatic signal at 1660-1750 cm^{-1} was enriched in the spots (Figure 9j), and so was the 1660 cm^{-1} shoulder. This spectral region may indicate the presence of aromatic carbonyls (Agarwal and Ralph, 1997; Taylor and Zografi, 1997). In contrast, the relative intensity of the major lignin doublet at 1590-1610 cm^{-1} and 1620-1630 cm^{-1} did not illuminate the spots (Figure 9f,h), and neither the shoulder at 1585 cm^{-1}. This indicates that generally, lignin is distributed evenly in the endodermis ITCW, however, benzoyl groups are enriched in a spotted pattern. In the roots treated with KI, we could not detect the spotted pattern by any mapping strategy (Figure 9e,g,i,k).

Lignin active deposition is required for the silica to aggregate

Aiming to test whether the lignin spots are required for the formation of silica aggregation, we exposed roots treated by KI to silicic acid. Three exposure schemes were compared: (1) Sorghum seedlings were grown for 1 week under Si- solution. After 1 week, the seedlings were pretreated for 2 hours with Si- & KI solution, and then moved to Si+ & KI for additional 12 hours. (2) Seedlings were grown under Si- & KI solution for 1 week, and then moved to Si+ & KI for 12 hours. (3) As control, we grew seedling in Si- solution, which were transferred after 1 week into Si+ for 12 hours (no KI was applied). In our hydroponics system, the basal 1 cm of the roots, closest to the root-shoot junction, was surrounded by a polystyrene foam plate that supported the seedlings. Therefore, this region of the roots was not exposed to the growing medium but to air. We monitored silica aggregation in mature root tissues, below and above the hydroponics solution (Figure 10). In the basal root part, never exposed to KI solution, silica aggregates developed regardless the treatment (Figure 10a,c,e). In the immersed parts of the root, the formation of aggregates under KI pretreatment was dramatically hindered compared to control roots (Figure 10b,d). Importantly, in this region, the ASZ lignin spotted pattern was fully developed, similarly to that in Si- roots. In roots cultivated with KI the entire growing period, aggregates were missing altogether (Figure 10f). Collectively, our results suggest that deposition of lignin in the spotted pattern is activated by apoplastic H_2O_2 and that silica aggregates onto these spots only a short time after their formation.

Discussion

Silica deposits require an optimal level of H_2O_2

In sorghum roots, silica aggregates are deposited in a neatly ordered pattern as part of the endodermal ITCW. This process is only attained by live tissue and is metabolically controlled (Soukup et al., 2019). Damaging the root locally prevented the formation of aggregates next to the wound, possibly as a result of cell death at the endodermis (Figure 3). The region lacking silica aggregates is larger than the wound itself. This may suggest that silica does not form also in live cells that sense a strong stress. Here we showed that excess H_2O_2 concentration is negatively correlated to the aggregate footprint, with highest effect at the lowest concentration tested (Figure 5). Aggregates were much bigger below the wound, as compared to above it (Figure 4). As the apoplastic H_2O_2 moves up the root with the transpiration stream, this trend may also reflect a stronger effect of a small increase in H_2O_2 concentrations. The complex relationship between ROS balance and silica deposition is in accord with the dual role of ROS in redox biology, that at low concentration induces cell proliferation, differentiation and elongation, and at high concentration signals for stress and cell death, and may apply stress via oxidation of useful molecules (Tsukagoshi et al., 2010; Schieber and Chandel, 2014). Nonetheless, under very low endogenic H_2O_2 concentration, during KI treatments, no aggregations formed (Figure 5). Since the tissue still contained lignin (Figure 8,9), it appears that a minimal level of H_2O_2 is required for the regular patterning of the aggregation sites.

Low H_2O_2 concentration reduces hemicellulose cross-linkage

Under KI treatments, the composition of the bulk cell wall was insignificantly altered. However, the hemicellulose pyrolysis temperature was lower by 16°C (Figure 8). Such decrease in thermal stability may be a result of reduced levels of cross linking (Farhat et al., 2017). Hemicellulose polymers are cross-linked to one another through di-ferulic acid ester bonds and to lignin by ester or ether bonds of ferulic or coumaric acid (Hatfield et al., 2017). In maize cell culture, exogenous H_2O_2 treatment leads to increased cross-linkage of the hemicellulose by ferulic acid, monolignols, and other phenylpropanoids (Fry et al., 2000). Further, the random nature of these bonds may increase the variability of hemicellulose pyrolysis temperature, which is 10 times higher in the control samples as compared to the samples grown under KI (Figure 8). In contrast, the pyrolysis of lignin was similar between the treatments, suggesting that lignin cross-linkage was not altered (Stewart et al., 1997).

The level of hemicellulose cross linking may appear in the Raman micro-spectroscopy as a shoulder in 1585 cm^{-1}, representing aromatic vibration, which is at 1600 cm^{-1} for unmodified phenylpropanoids bound in lignin (Agarwal and Ralph, 1997). Such red shift indicates modifications on the aromatic ring

that result in extended pi-system, possibly by dimerization with another aromatic ring (Nuopponen et al., 2004; Abraham et al., 2018). Since mapping of spectral regions containing the 1585 cm^{-1} shoulder did not show the spotted pattern (Figure 9), we conclude that hemicellulose and its modifications does not form nucleating centers for silicic acid. This is in accordance with our previous results, based on chemically treated endodermis samples (Zexer and Elbaum, 2020). In contrast, the shoulder at 1660 cm^{-1} did map to the spots, suggesting aromatic carbonyl modifications on the ASZ lignin (Agarwal and Ralph, 1997; Taylor and Zografi, 1997). The incorporation of carbonyl residues into lignin is increased under reduced activity of cinnamyl alcohol dehydrogenase (CAD), (Stewart et al., 1997). Similarly, a mutation in CAD that causes a brown mid-rib phenotype in the *Sorghum bicolor* mutant *bmr6* (Sattler et al., 2009), possibly increases the fraction of aldehydes in the lignin (Yahiaoui et al., 1997). Interestingly, in roots of sorghum *bmr6* mutant the silica aggregate footprint was larger by 70% than that of wild type aggregates (Figure S1). Our results strongly indicate that the ASZ lignin is enriched with carbonyl groups conjugated to aromatic rings. These modifications may nucleate silicic acid in the roots of sorghum.

Silica deposits on lignin that is polymerized in reaction to H_2O_2 activity

The lignin spotted pattern developed in plants starved for silicic acid, similarly to the silica aggregation pattern in plants fed with silicic acid (Figure 7), (Zexer and Elbaum, 2020). This means that the ASZ lignin deposition is independent of silicic acid. In contrast, in roots treated by KI, no ASZ lignin nor silica deposited. A hierarchical relationship appears, in which H_2O_2 is required for the formation of lignin that is needed for silica aggregation.

When the formation of lignin was arrested concurrently with the application of silicic acid, normal silica aggregation occured in region IV (Figure 5f). This suggests that the tissue was ready for the nucleation of silicic acid before the arresting of lignin formation. In contrast, the similar root region under similar growing conditions did not nucleate silicic acid when it was pretreated by KI for 2 hours (Figure 10d). This result indicates that the spots of ASZ lignin, deposited before the KI treatment, were not active in nucleating the silicic acid. This implies that the ASZ lignin can nucleate silica aggregation only during a short window of time after its deposition. Further, once silica started to form, the aggregate will continue to grow independently of the lignin polymerization (Figure 5f).

ASZ lignin deposition may be patterned by localized secretion of modified monolignols

Lignin formation requires a source for radicals. These could be oxygen molecules processed enzymatically by laccases. Alternatively, NADPH oxidase (called respiratory burst oxidase homologs (RBOH) in plants) produces $O_2^{-\cdot}$ that are converted to H_2O_2 molecules, processed by peroxidases. A

radical is transferred by the enzymes to a phenylpropanoid, which is coupled to a growing lignin polymer. In Arabidopsis, lignin deposition is patterned by the formation of enzyme complexes bound to the cell wall under specific developmental contexts, such as lignification of xylem elements or root Casperian strips (Lee et al., 2013; Hoffmann et al., 2020). The enzyme complexes include anchoring motifs, RBOHs, superoxide dismutase (SOD), and laccases or peroxidases. In our system, we find profound influence of apoplastic H_2O_2 concentration on the intensity of localized lignification. This suggests the involvement of peroxidases in the tertiary cell wall formation. Further, the lignification pattern was not altered under the H_2O_2 treatments, suggesting that the endogenous production of H_2O_2 does not control the lignin patterning. Therefore, the pattern could originate from a pattern of peroxidases bound to the cell wall, or by modified monolignols (typical to ASZ lignin) that are in some way concentrated in the spots. Lignification occurs over the whole surface of the tertiary cell wall, with lower deposition in the spots, as seen by mapping the Raman total lignin scattering (Figure 9d,e). This suggests the activity of peroxidases and / or laccases throughout the ITCW. The total lignin formation was only non-significantly altered by KI treatments and quenching of H_2O_2 (Figure 8). We may assume that the lignin forming in the seedling root is mostly produced as a result of laccases activity, unaffected by altered levels of H_2O_2. This may suggest that the ASZ lignin pattern forms by patterning of peroxidases on a background of laccases. However, both laccases and peroxidases will interact with whatever lignin monomers they may find, including the ASZ lignin monomers. Therefore, our results strongly suggest that the spotted pattern of lignin modified by conjugated carbonyls must originate from patterned secretion of ASZ-phenylpropanoid monomers, possibly aldehydes (Sattler et al., 2009). We suggest a model in which the ASZ lignin monomers are secreted by the cell near bound complexes of RBOH and peroxidases. Since the monolignols can diffuse freely in the cell wall, their binding into the growing lignin polymer must be very rapid. Once bound, they interact with silicic acid molecules to nucleate a rapidly growing silica aggregate. The complexes migrate to the rims of the aggregate and increase its footprint (Figure 2h). If silicic acid is not available, the ASZ lignin monomers bind to the wall via the activity of peroxidases and H_2O_2 to form spots (Figure 2g). The lignin carbonyl modifications may allow for tight crosslinking of the cell wall, causing spots of high density (Figure 9d). Once cross-linked, the ASZ monomers are unavailable for nucleating the silica aggregates. Under KI treatment and low H_2O_2 concentration, the peroxidases clusters are inactive. The ASZ lignin monomers diffuse away from their secretion location and couple to the bulk ITCW by the activity of lacasses.

Can Si availability alter stress signaling through modulation of ROS?

Silicon in plants is studied as a stress-ameliorating agent. Reports encompass species from diverse plant families confronting a range of both biotic and abiotic stresses (Liang et al., 2007; Van Bockhaven et al., 2013; Coskun et al., 2019). Many of these works point to Si-generated effects on plants' oxidative state including gene regulation, protein abundance and ROS levels (Cooke and Leishman, 2016), first suggested by (Chérif et al., 1994). A specific example in root endodermis shows that the supplementation of silicic acid to the growing medium enhances lignification (Fleck et al., 2011; Lukačová et al., 2013) but not suberization (Kreszies et al., 2020) through modulation of ROS and ROS-dependent enzymes (Fleck et al., 2011). In this work, we show a reciprocal effect: The apoplastic oxidative levels affect the extent of endodermal silicification in roots of sorghum seedlings through mediation of lignin formation. A feedback mechanism can be contemplated, between Si and cell wall oxidative levels. Once silicic acid is available for the tissue, ASZ lignin polymerization at the silica aggregation loci seems to be restricted. Both ASZ lignin monomers and H_2O_2 diffuse away from the silicification locus. Under these conditions, the H_2O_2 molecules may initiate signaling cascades in the protoplast (Neill et al., 2002; Mittler et al., 2004). Such mechanism would affect the tissues oxidative homeostasis, potentially altering signaling and perception of stress conditions. Further research may reveal a direct link between the formation of silica and ROS-related stress.

Materials and Methods

Plant material and growth conditions

Grains of *Sorghum bicolor* (L.) Moench, line BTx623 were surface-sterilized with 3% sodium hypochlorite for 10 min and rinsed twice with distilled water. Grains were then placed in petri dishes lined with wet filter papers and germinated for 72 h. After germination, seedlings were grown hydroponically for one week. All growth solutions were based on double distilled water containing 1 mM $CaCl_2$. Si+ medium was supplemented with sodium silicate (Na_2SiO_3) at a final concentration of 2 mM. Si- medium was supplemented with NaCl at a similar final concentration in order to maintain equal ionic balance across all media. The final pH of all the solutions was adjusted to 5.8 with HCl. In relevant experiments, NaCl, KI and H_2O_2 (Sigma-Aldrich) were added to the solutions. Seedling were grown on plates of polystyrene foam mounted on top darkened 1 L beakers containing growing media. In each beaker we grew ten seedlings. Cultivation was done in a growth chamber, under controlled conditions with photoperiod 16 h : 8 h (light : dark) illuminated with photosynthetic active radiation (PAR) of approximately 200 μmol m^{-2} s^{-1}, at a temperature of 28°C : 22°C (light : dark), and 70% air humidity.

Root tissue fixation

Complete primary roots were harvested and fixed in ethanol : acetic acid (9:1 v/v) under vacuum for 24 hours. Root samples were kept in the same fixative at 4°C for additional 48 hours. The fixing solution was then replaced with ethanol 70% and samples were stored at 4°C until use.

3,3'-diaminobenzidine (DAB) staining and roots sectioning

DAB staining was preformed according to (Daudi and O'Brien, 2012) with minor changes. Briefly, complete excised primary roots were immersed in petri dishes containing freshly made DAB aqueous solution (5.2 mM, Sigma-Aldrich). Appropriate infiltration of the stain was ensured by applying gentle vacuum for 5 min using a desiccator. Petri dishes were then covered with aluminum foil and placed on a laboratory shaker. After 5 hours of gentle shaking, root samples were transferred to ethanol : acetic acid (9:1 v/v) fixative solution. The solution was replaced once and followed by the fixation procedure described earlier.

Three-millimeter long root sections were rinsed with double distilled water, positioned in plastic molds, and embedded in O.C.T embedding compound (Scigen, USA). The molds were carefully lowered into liquid nitrogen until the O.C.T medium froze. A CM1860 cryostat (Leica) was used to cut 20 µm thick sections, which were mounted on glass slides. These were observed and photographed with a Leica DM500 microscope equipped with an x40 objective and coupled to a Leica ICC50W camera.

Aggregate assessments by scanning electron microscopy (SEM)

Fixed root samples were carefully peeled out of their cortical tissues using finely serrated tweezers. Representative segments of each sample were mounted on aluminum stubs using carbon tape. Observations were performed with a JEOL JSM-IT 100 InTouchScope^{TM} scanning electron microscope (SEM), (JEOL, Japan) under low vacuum (30 Pa) and with accelerating voltage of 20 kV. All micrographs were taken using the back scattered electrons mode. Aggregates footprint were measured by analysis of the SEM micrographs using ImageJ2 software (Schneider et al., 2012).

Phloroglucinol-HCL staining

Staining solution was prepared by mixing a 3% Phloroglucinol (Sigma-Aldrich) solution in ethanol (100%) (w/v) followed by the addition of 0.5 volume of hydrochloric acid (32%). The cortex of fixed roots was removed. Desired segments were hand-cut from each root and mounted on glass slides using freshly made staining solution. Slides were immediately observed and photographed with a Leica DM500 microscope equipped with an x40 objective and a Leica ICC50W camera (Leica, Germany).

Estimation of the distance from root tip to the active silicification zone (ASZ)

The distance of silica aggregates and lignin spots from the root tip was measured according to the tissue autofluorecence (see Zexer & Elbaum, 2020b). The cortex of complete and fixed roots was removed. The exposed stele of each root was cut to 1 cm long pieces, starting at the root tip and keeping their order up to the root basal end. Sections were then mounted on glass microscope slide using distilled water. The autofluorescence pattern of blue spots (in Si+ roots, (Soukup et al., 2014) or green spots (in Si- roots, (Zexer and Elbaum, 2020) was tracked from the basal section of the roots until no spots could be identified. We recorded the length from the tip of each root to this section. Observations were performed using a Nikon Eclipse 80i microscope (Nikon, Japan) and an X-cite 120Q (Lumen Dynamics, Canada) UV light source. Specimens were observed using an x20 Nikon lens with the following set of Nikon filters: GFP (excitation: 450–490 nm; emission: 500–550) and DAPI (excitation: 400–418 nm; 450–465 nm).

Thermogravimetric analysis (TGA)

Peeled primary roots were ground into fine powder using liquid nitrogen and a mortar and pestle (30 roots per sample). The crushed tissue was then dried at 65°C for at least 72 hours before use. Ground and dried samples (16-20 mg) were mounted on platinum pans and measured using a Q500 thermogravimetric analyzer (TA instruments, USA). Pyrolysis was performed in a nitrogen atmosphere and heating ramp of 15°C / min from room temperature up to 900°C. Calculation of the differential thermal gravimetric (DTG) graphs was done using the Universal Analysis 2000 software (TA instruments, USA). The relative quantification of the cell wall polymers was calculated by fitting peaks to the DTG graphs and recording the area underneath the fitted decomposition peaks by WiRE3.2 software (Renishaw, New Mills, UK).

Raman micro-spectroscopy

Root segments were prepared as described for the aggregate assessments by SEM, and mounted on aluminum microscope slides using super glue. The samples were covered with a drop of double-distilled water and measurements were made using an x63 water-immersed objective. Raman maps were collected with a Renishaw InVia spectrometer equipped with a 532 nm laser (45 mW maximum intensity), utilizing WiRE3.2 software (Renishaw, New Mills, UK). Measurements were performed by using the Streamline mode with acquisition time of 30 sec. Maps were composed of between 3000 and 5000 spectra with steps of 1 μm in the x direction. Spectral analysis was done in WiRE3.2 (Renishaw), including peak picking, first derivative calculation, and signal ratio mapping.

Statistics

Statistical analysis was preformed using JMP statistical package version Pro15 (JMP®, SAS institute Inc., USA). Statistical significance was assumed at $P \leq 0.05$. For the comparisons of aggregates footprints area, in each treatment at least three roots were used and three micrographs from each root were analyzed (n = 600-1500 aggregates). For measurements of distances form the root tip to the ASZs, at least three roots per treatment were used. The data were subjected to ANOVA followed by the Tukey-Kramer post-Hoc test.

Acknowledgements

The research was funded by the Israeli Ministry of Agriculture & Rural Development, Chief Scientist Office grant 12-01-0016. N.Z is thankful to the Robert H. Smith Foundation for a scholarship.

Figures

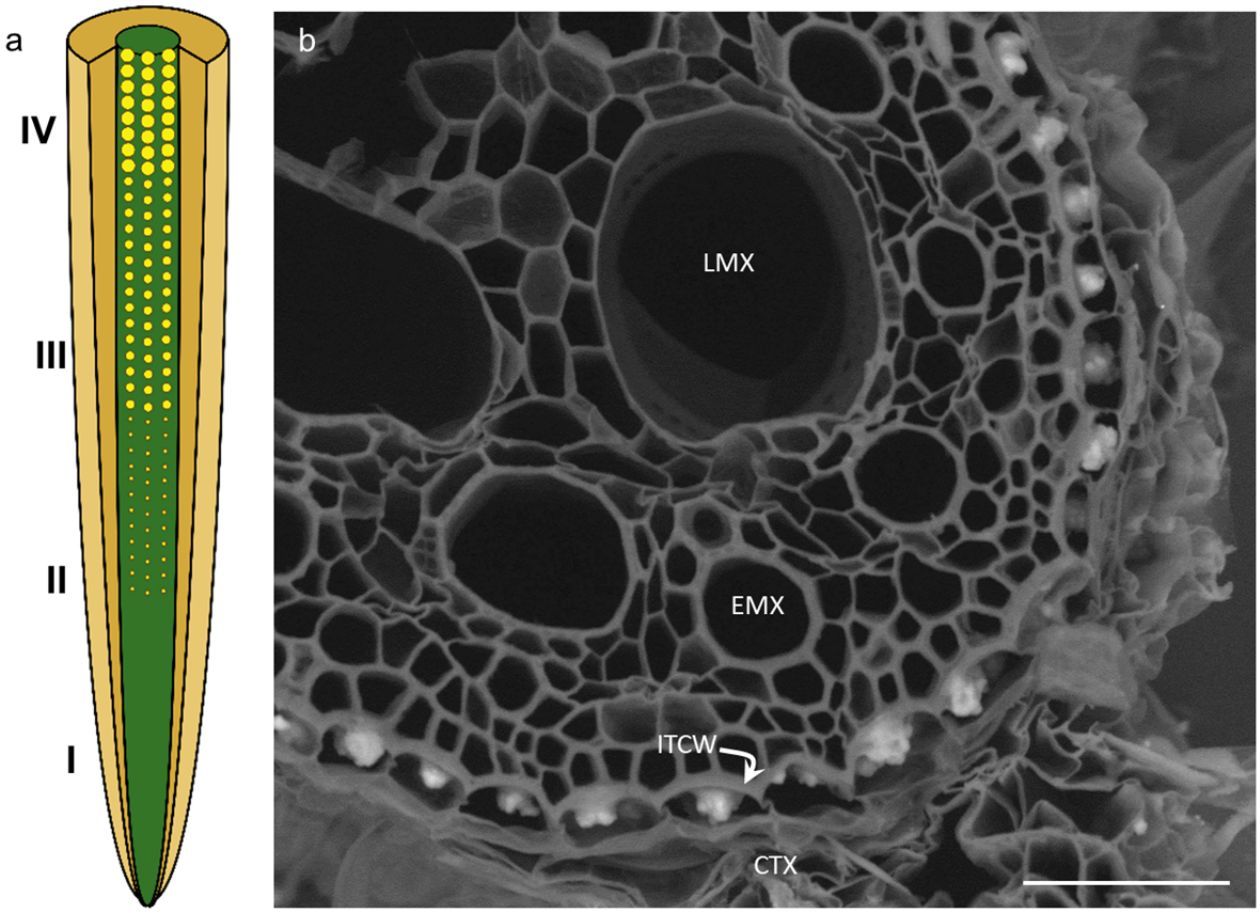

Figure 1. Silica aggregation along the endodermis of a sorghum (*Sorghum bicolor* L.) seedling primary root. (a) Schematic diagram of a seminal root, drawn without lateral roots (not to scale). In green we represent the central cylinder and in brown the cortex. The endodermis is a single cell layer that resides between these two tissues. Silica aggregates (yellow circles) develop on the inner tangential cell wall (ITCW) of the endodermis. No aggregates are found at the root tip and up to about 4-6 cm (region I). Aggregation is initiated at about 4-5 cm from the root tip (region II). The aggregates grow in diameter and height along their maturation in regions III and IV. (b) Scanning electron micrograph of a cross section in region IV of a sorghum seedling primary root. The central cylinder shows early (EMX) and late meta-xylem (LMX) vessels. The cortex (CTX) was mostly removed. The thick endodermis ITCW (ITCW) is shown with highly bright silica aggregates. Scale bar represents 50 µm.

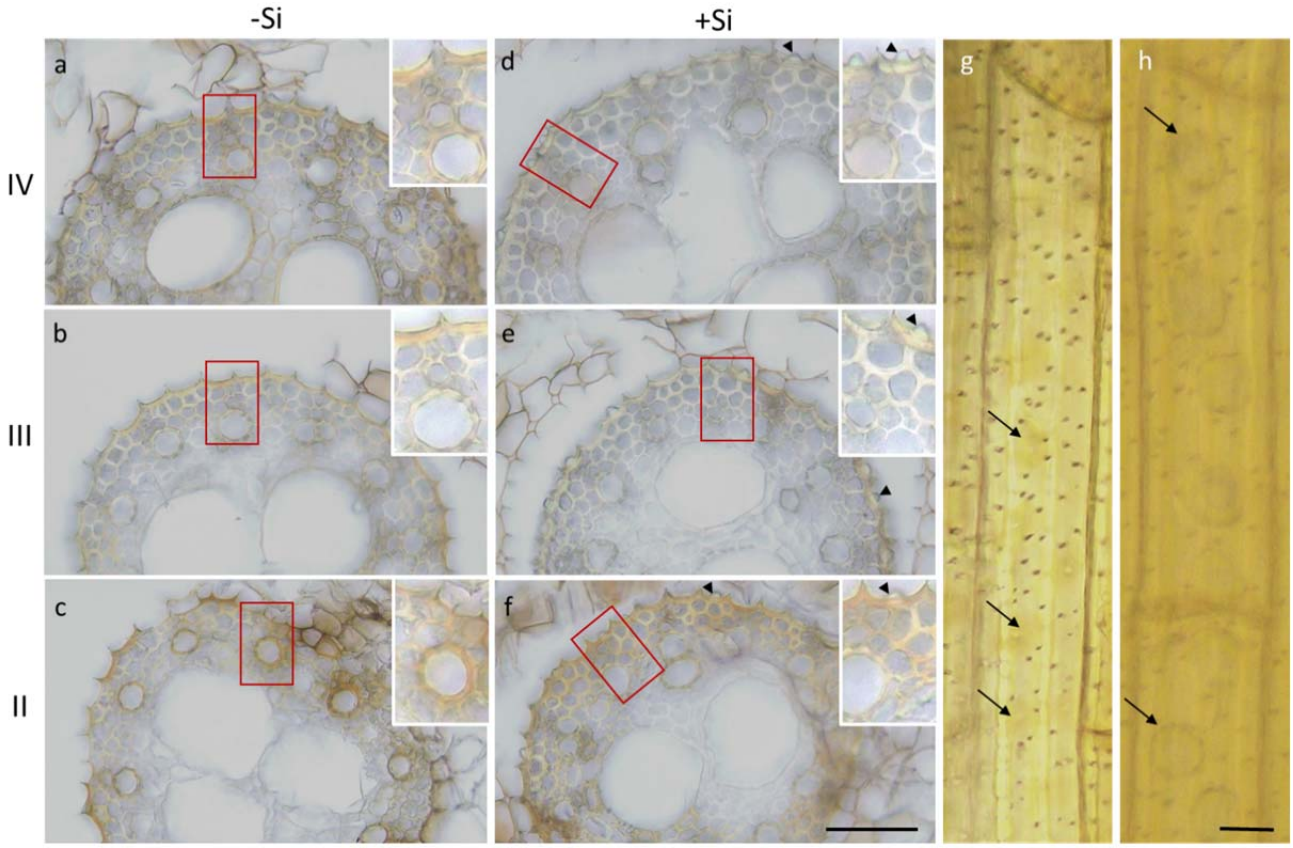

Figure 2. Primary roots of sorghum seedlings stained with 3,3'-diaminobenzidine (DAB). Cross sections taken from a Si- (a-c) and a Si+ root (d-f) represent regions IV, III, and II of silica aggregation along the root, as defined in Figure 1. Insets are enlargements of the red rectangles in each of the panels. Brown discoloration attributed to the precipitation of DAB can be seen in the endodermal ITCW and the cell walls of xylem elements in all three regions. The staining is more intense in region II of both treatments. This is the region of Si aggregation onset. Arrowheads indicate some silica aggregates. (g) A longitudinal view of DAB stained ITCW from a Si- root. Slightly stronger tainted spots (arrows) can be seen on the background of the stained cell wall. Pits are seen as dark dots. (h) A similar longitudinal view of a Si+ ITCW. The outlines of Si aggregates are evident in darker stain (arrows) on the uniformly stained ITCW. Scale bar in f, common to a-f represents 50 µm. Scale bar in h, common to g and h represents 5 µm.

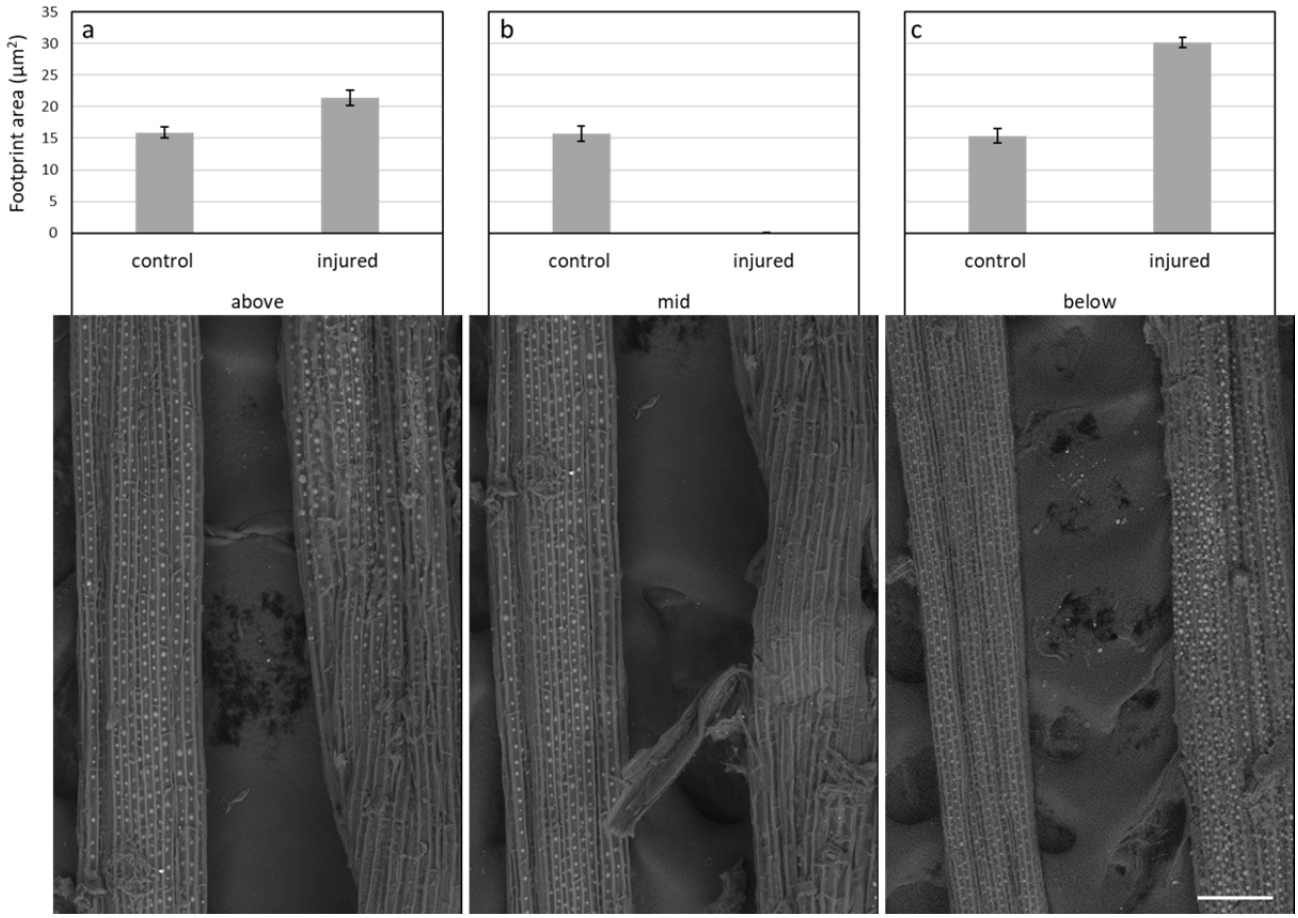

Figure 3. The effect of local injury on silica aggregates footprint. Bottom panels show scanning electron micrographs of an uninjured root (left) and a root locally injured using a needle (right). Above each micrograph is a graph of the measured mean footprint of the aggregates. Bars represent standard error. Variations between the treatments are statistically significant. (a) In the region about 0.5 mm above the injury, the aggregates that formed in the injured root were larger than aggregates in the uninjured root. (b) No aggregates were found around the injured area. (c) In the region about 0.5 mm below the site of injury, the aggregates that formed in the injured root were larger than aggregates in the uninjured root. Scale bar in panel c, common to all micrographs, represents 100 µm.

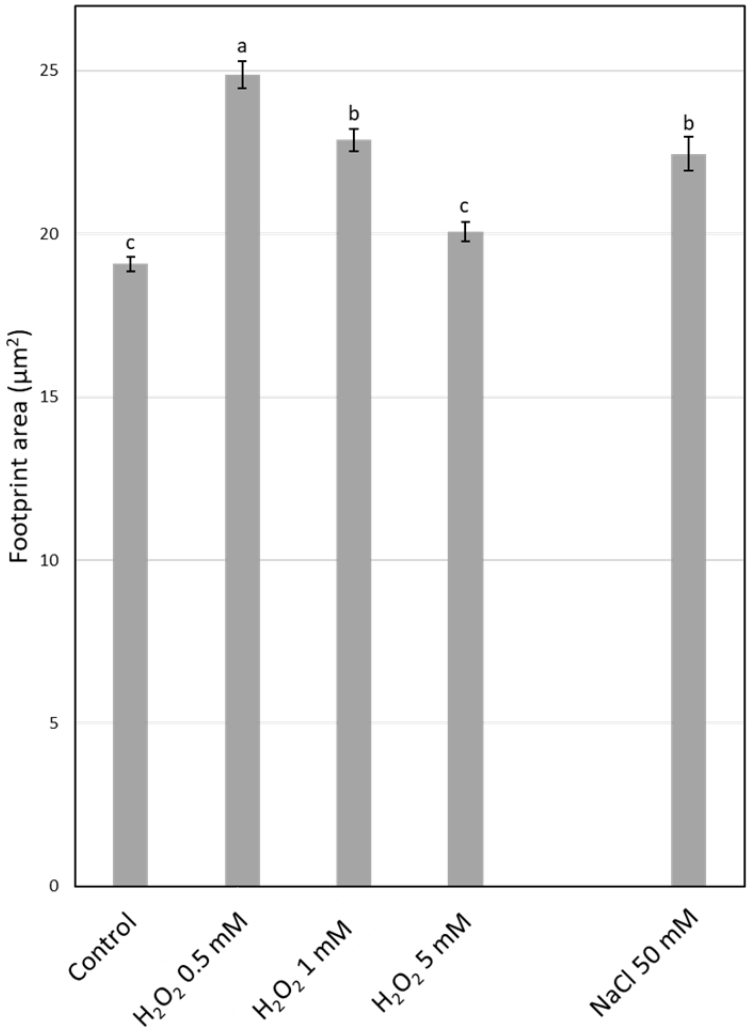

436 **Figure 4.** The effect of exogenous H_2O_2 and NaCl treatments on the average footprint of root silica
437 aggregates in the endodermal ITCW. Presented are mean aggregate areas and standard errors.
438 Treatment of 1 mM H_2O_2 resulted in an aggregate footprint 15% larger than aggregates in unstressed
439 (control) roots. Similar increase was measured under 50 mM NaCl stress. Bars represent standard
440 errors and different letters indicate significant differences at $P \leq 0.05$.
441

Figure 5. Silica deposition in the endodermal ITCW under high and low H_2O_2 regimes. Roots grown in Si- media for three days were transferred to Si+ (control), Si+ & 0.5 mM H_2O_2, and Si+ & 1 mM KI treatment media for additional four days. (a-c) Representative images of (a) control, (b) H_2O_2, and (c) KI treated roots. (d-f) Scanning electron micrographs of region IV of (d) control roots, and (e) H_2O_2, and (f) KI treated roots. (g-i) Scanning electron micrographs of region III of (g) control roots, and (h) H_2O_2, and (i) KI treated roots. (j-l) Scanning electron micrographs of region I of (j) control roots, and (k) H_2O_2, and (l) KI treated roots. In roots treated with H_2O_2, silica aggregates formed prematurely in region I. No aggregates developed in cells that completed their development under KI treatment. Scale bar in c, common to a-c, represents 1 cm. Scale bar in panel l, common to d-l, represents 50 µm.

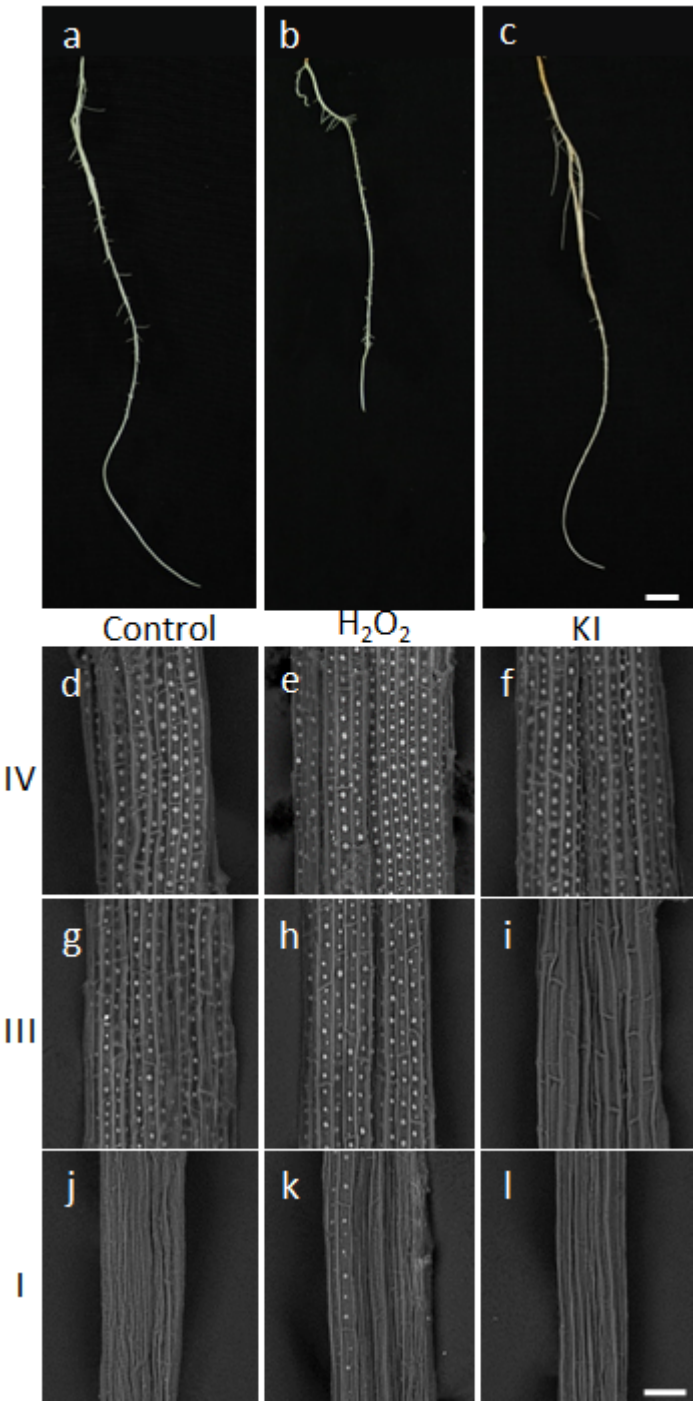

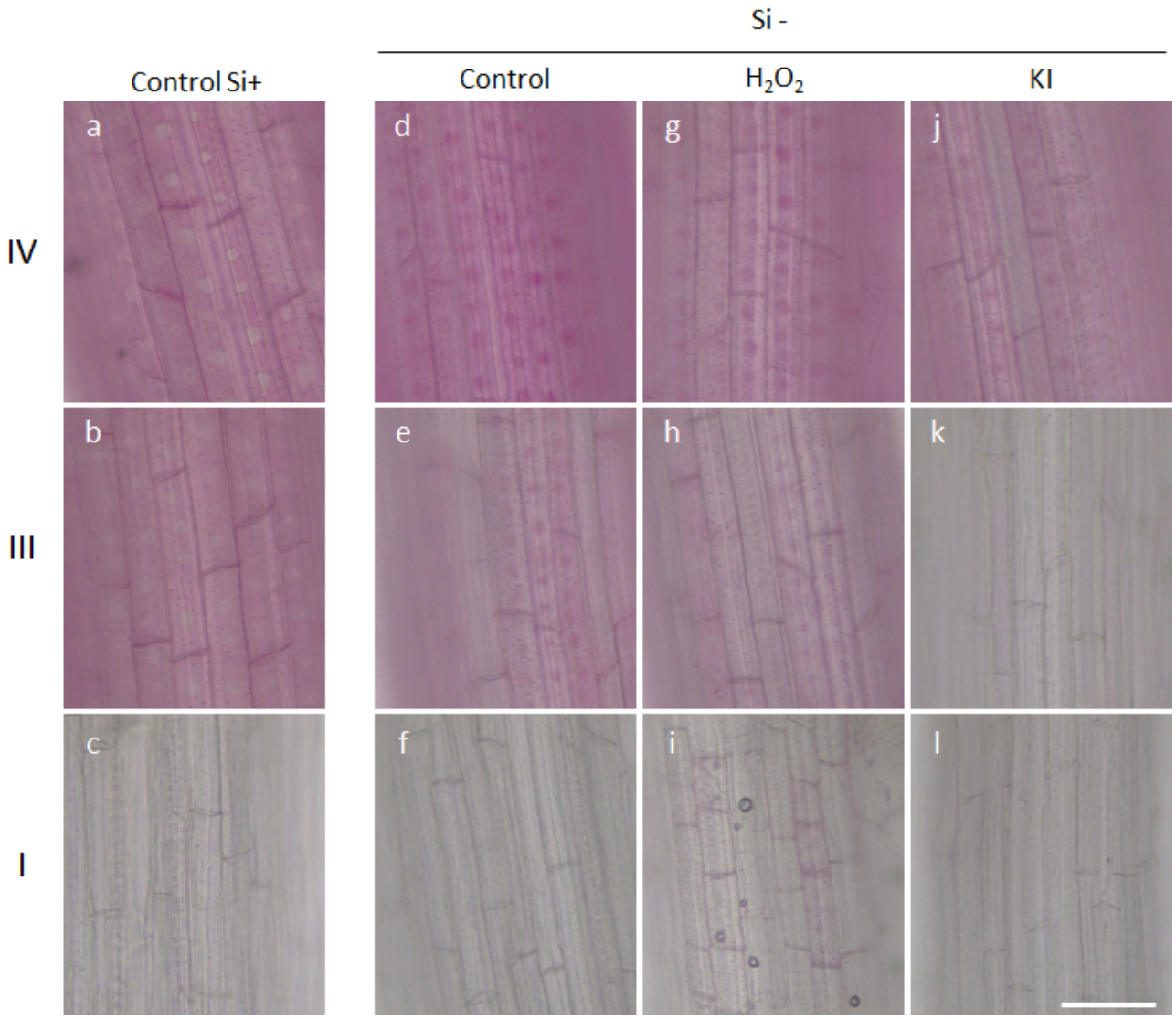

Figure 6. Lignin deposition in the endodermal ITCW under high and low H_2O_2 regimes. (a-c) Roots grown in Si- media for three days were transferred to Si+ media and stained for lignin with Phloroglucinol-HCl. Unstained silica aggregates are evident on the stained background of the ITCW in regions IV (a) and III (b). (c) There is no staining in region I. (d-l) Roots grown in Si- media for three days were transferred to Si- (control), Si- & 0.5 mM H_2O_2, and Si- & 1 mM KI treatment media for additional four days, and stained for lignin with Phloroglucinol-HCl. Optical micrographs were collected from control (d-f), H_2O_2 (g-i) and KI (j-l) treatments, in region IV (top panels), III (middle panels), and I (bottom panels). In roots treated with H_2O_2, deposits of lignin in spots formed prematurely in region I. Lignin spots are not detected in cells that completed their development under KI treatment. Scale bar in l, common to all panels represents 50 µm.

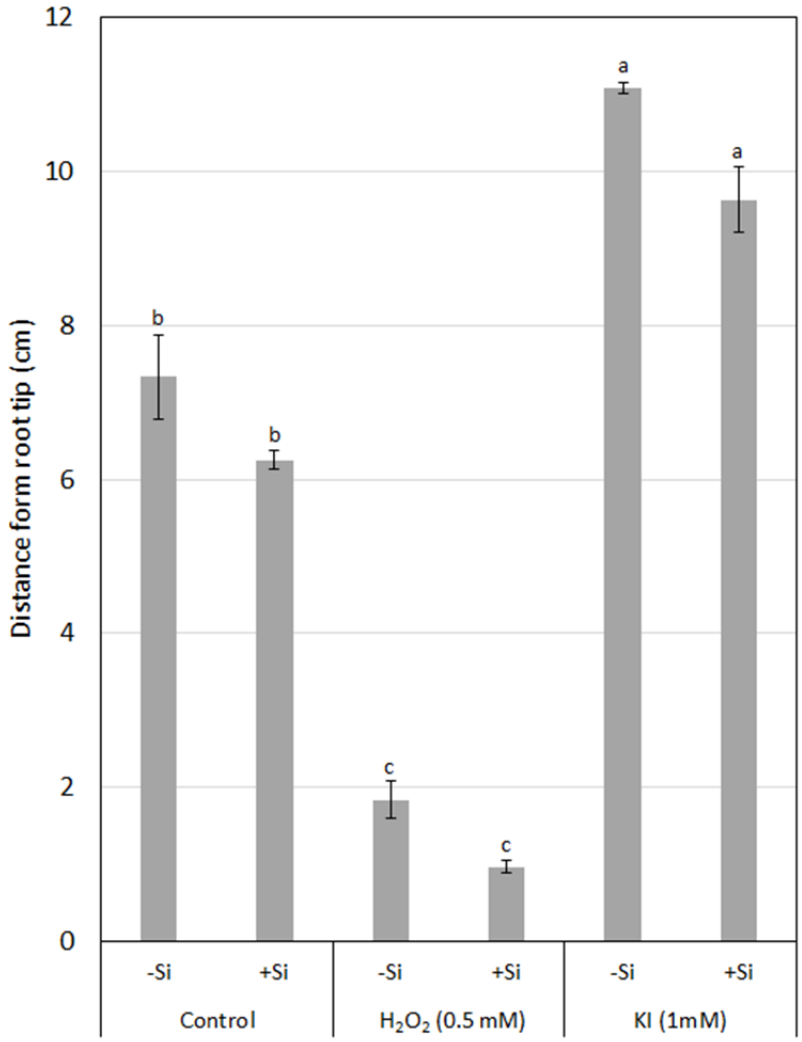

474 **Figure 7.** Location along the root of initial silica aggregation (in Si+ roots) or lignin spotted pattern (in
475 Si- roots). The average distance from the root tip to the first autofluorescent spot is plotted in control,
476 H_2O_2, and KI treated roots. Bars represent standard error. Different letters indicate significant
477 differences at $P \leq 0.05$.
478

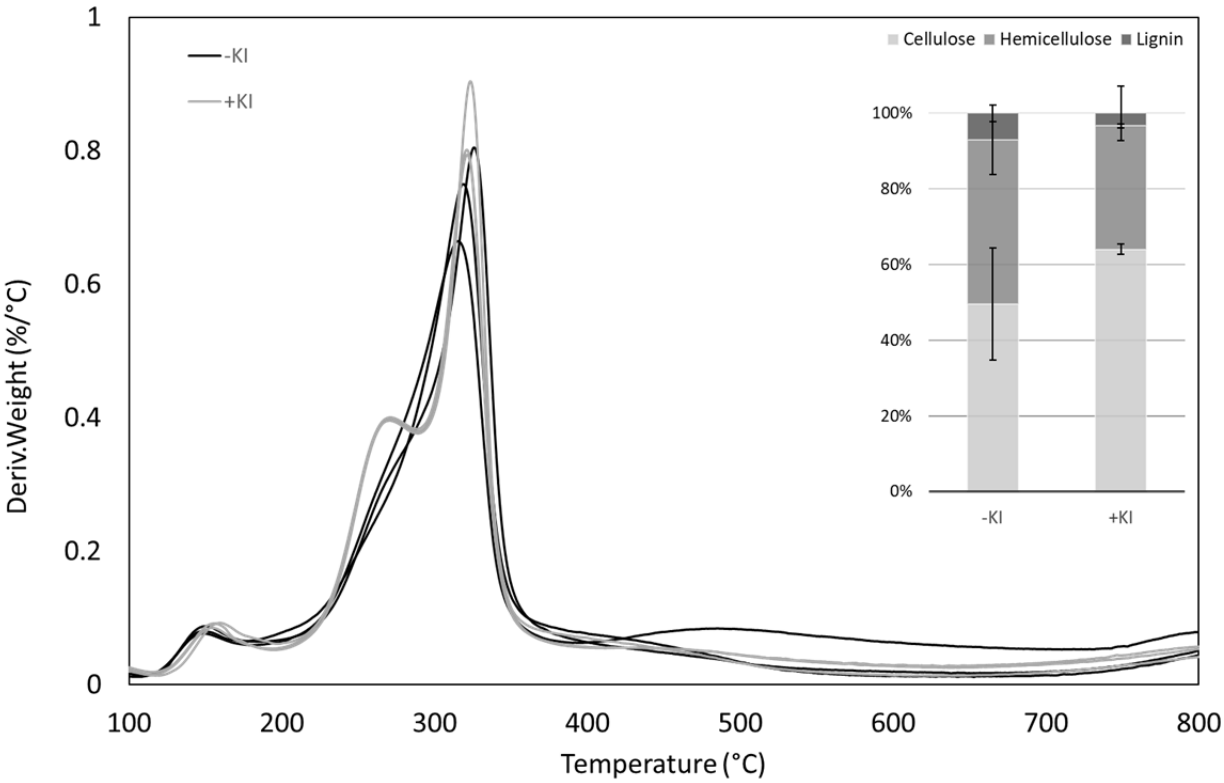

Figure 8. Differential thermal gravimetric analysis of Si- roots grown under control (black) or 1 mM KI (gray) treatment. Three biological repetitions were measured for each treatment. Inset bar graph shows the relative average fraction and standard deviation of cellulose, hemicellulose and lignin calculated by peak fitting at about 311 - 323°C, 266 - 283°C, and 390 - 480°C respectively.

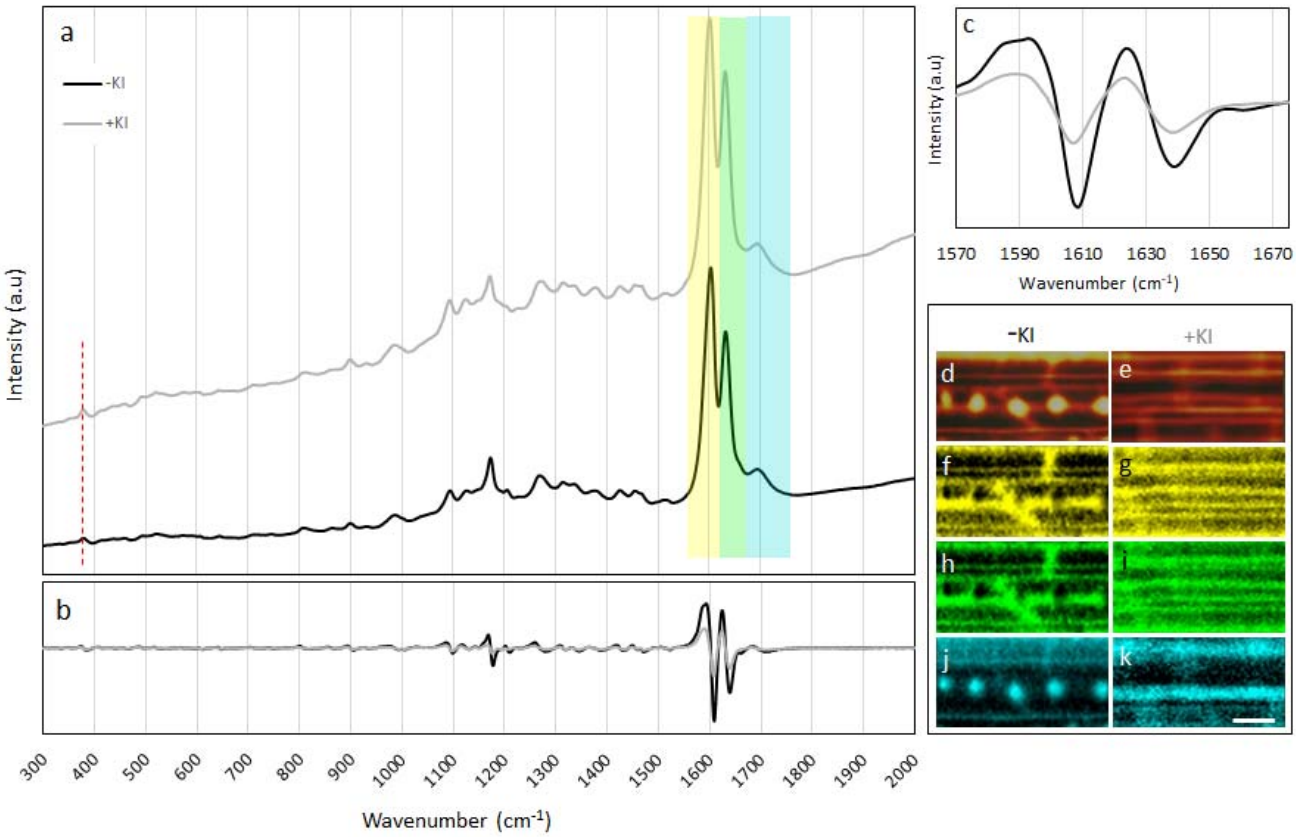

Figure 9. Raman micro-spectroscopy of endodermal ITCW in Si- roots grown under control or KI (1 mM) treatment. (a) Average spectra of ITCW maps of control (black) and KI (gray) treated roots. The colored rectangles indicate spectral regions mapped in panels f-k, normalized to the crystalline cellulose peak at 378 cm^{-1} (red dashed line). (b) First derivative of the average spectra in panel A. (c) Enlargement of the spectral range 1570-1675 cm^{-1} in panel B. (d-e) Maps of the total Raman signal measured from the ITCW of (d) control and (e) KI treated roots. (f-k) Maps depicting typical lignin signals normalized to the crystalline cellulose peak at 378 cm^{-1} of control (left) and KI (right) treated roots. (f-g, yellow) 1550-1618 cm^{-1}, (h-i, green) 1618-1660 cm^{-1}, (j-k, cyan) 1660-1750 cm^{-1}. Scale bar in k, common to d-k, represents 20 µm.

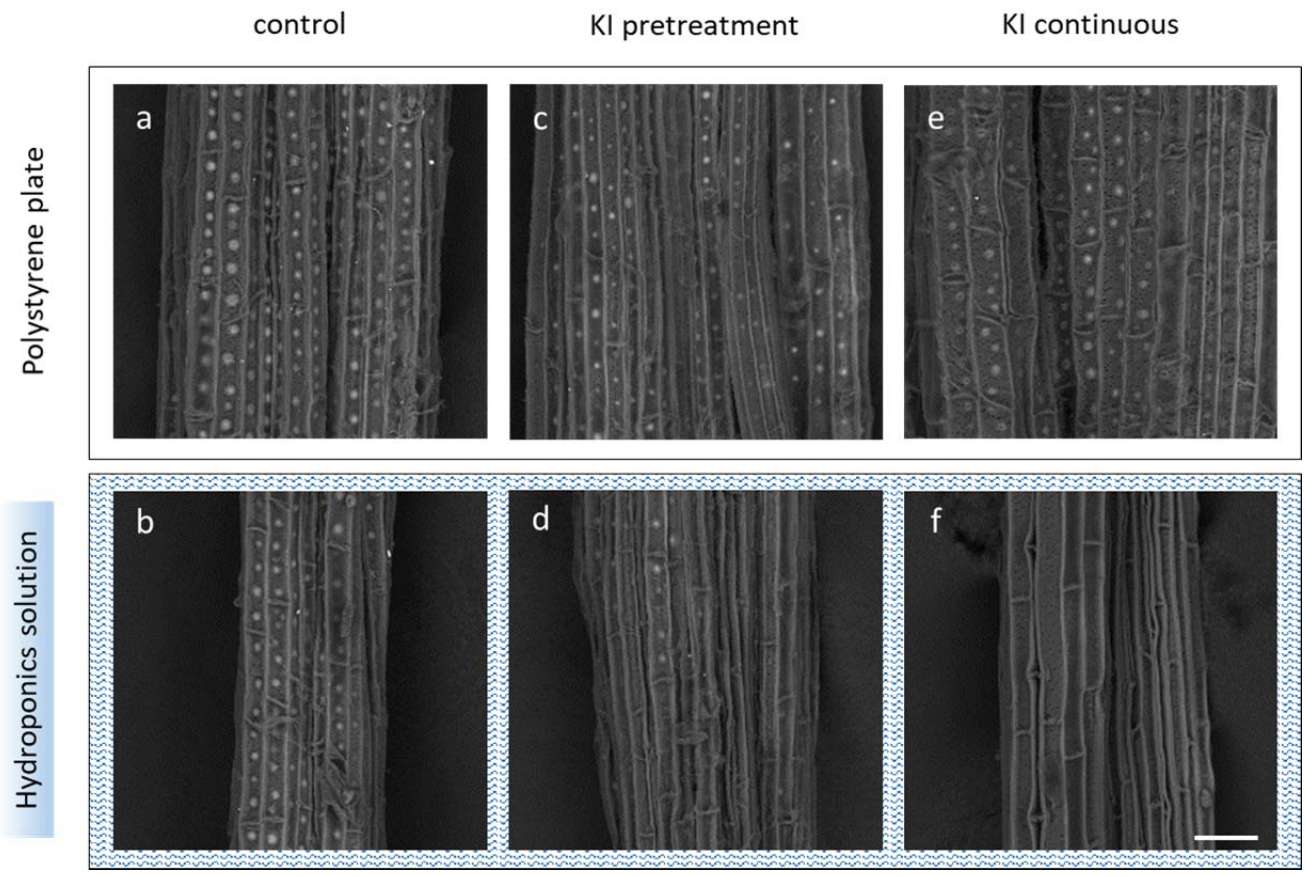

Figure 10. The effect of KI 2-hour pretreatment and KI continuous treatment on the formation of silica aggregates, depicted by scanning electron microscopy. (a,b) Roots were grown under Si- for 3 days and then moved to Si+ medium for another 3 days (control). (c,d) Roots grown in Si- solution were pretreated by KI and then moved to Si+ & KI for another 3 days (KI pretreatment). (e,f) Roots grown in Si- solution were moved to Si+ & KI treatment for another 3 days (KI continuous). (a,c,e) Micrographs of root sections from the basal end. This root part was not in contact with the hydroponics solutions. (b,d,f) Micrographs of mature root tissues in region IV that were immersed in the hydroponics solutions. Scale bar in f, common to all panels, represents 50 µm.

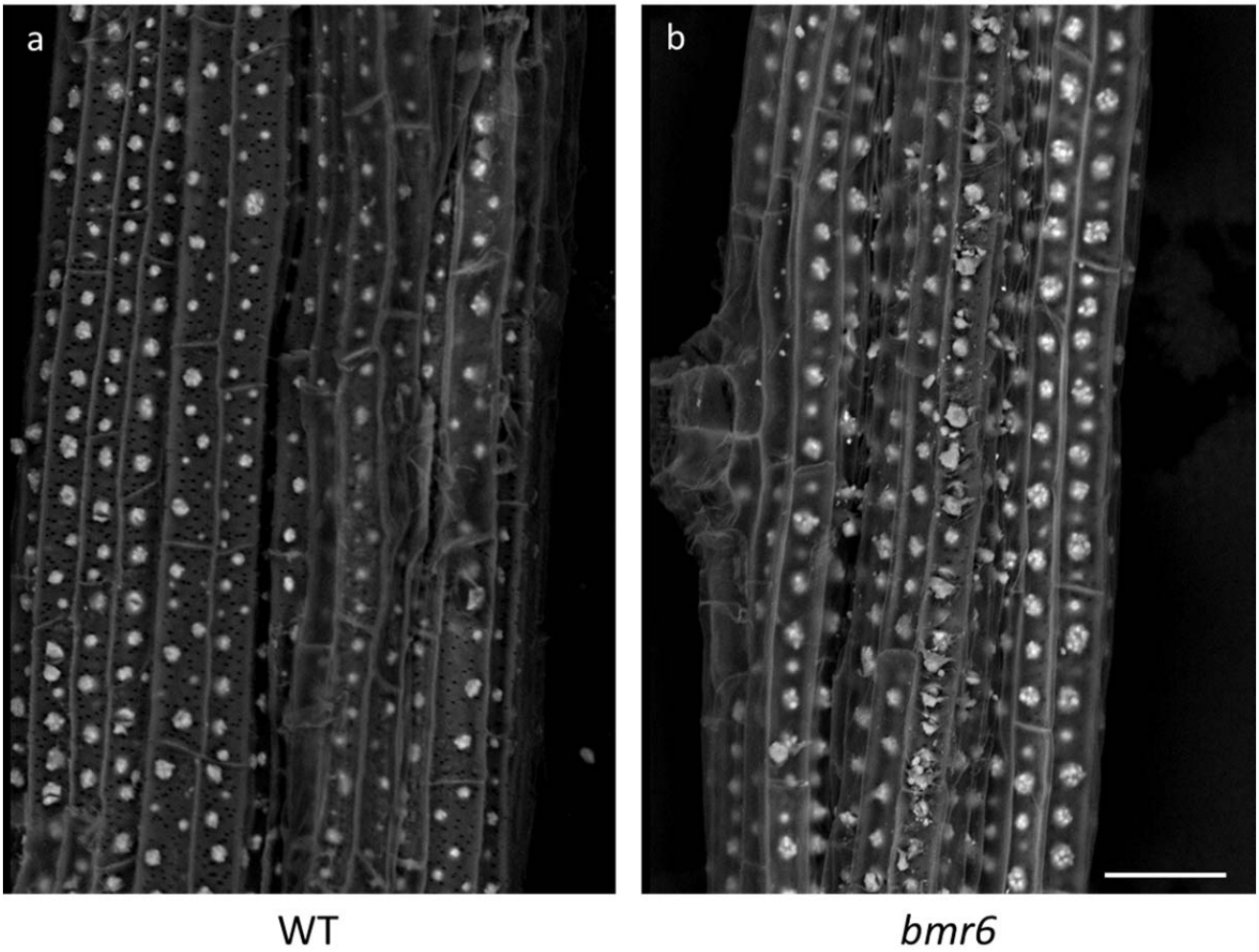

Figure S1. Silica aggregates formation in region IV in sorghum (a) wild-type (WT) and (b) *bmr6* roots. The *bmr6* genetic stock is PI639713, obtained from the USDA. Scale bar common to both panels represents 50 µm. Average aggregate footprint area were significantly different between the genotypes. We measured mean footprints (± SE) of 24 ± 5 μm^2 in the wild-type plants and 39 ± 9 μm^2 in the *bmr6* mutant plants.

510

Parsed Citations

Abraham Y, Dong Y, Aharoni A, Elbaum R (2018) Mapping of cell wall aromatic moieties and their effect on hygroscopic movement in the awns of stork's bill. Cellulose 25: 3827–3841
Google Scholar: Author Only Title Only Author and Title

Agarwal UP (2014) 1064 nm FT-Raman spectroscopy for investigations of plant cell walls and other biomass materials. Front Plant Sci 5: 490
Google Scholar: Author Only Title Only Author and Title

Agarwal UP, Ralph SA (1997) FT-Raman Spectroscopy of Wood: Identifying Contributions of Lignin and Carbohydrate Polymers in the Spectrum of Black Spruce (Picea mariana). Appl Spectrosc, AS 51: 1648–1655
Google Scholar: Author Only Title Only Author and Title

Barceló AR (1995) Peroxidase and not laccase is the enzyme responsible for cell wall lignification in the secondary thickening of xylem vessels inLupinus. Protoplasma 186: 41–44
Google Scholar: Author Only Title Only Author and Title

Bennett DM (1982) An ultrastructural study on the development of silicified tissues in the leaf tip of barley (Hordeum sativum jess). Ann Bot 50: 229–237
Google Scholar: Author Only Title Only Author and Title

Casey WH, Kinrade SD, Knight CTG, Rains DW, Epstein E (2004) Aqueous silicate complexes in wheat, Triticum aestivum L. Plant, Cell & Environment 27: 51–54
Google Scholar: Author Only Title Only Author and Title

Chérif M, Asselin A, Bélanger RR (1994) Defense responses induced by soluble silicon in cucumber roots infected by Pythium spp. Phytopathology 84: 236–242
Google Scholar: Author Only Title Only Author and Title

Cooke J, Leishman MR (2016) Consistent alleviation of abiotic stress with silicon addition: a meta-analysis. Funct Ecol 30: 1340–1357
Google Scholar: Author Only Title Only Author and Title

Coskun D, Deshmukh R, Sonah H, Menzies JG, Reynolds O, Ma JF, Kronzucker HJ, Bélanger RR (2019) In defence of the selective transport and role of silicon in plants. New Phytologist 223: 514–516
Google Scholar: Author Only Title Only Author and Title

Daudi A, O'Brien JA (2012) Detection of hydrogen peroxide by DAB staining in Arabidopsis leaves. Bio Protoc 2: 1–4
Google Scholar: Author Only Title Only Author and Title

Elbaum R, Melamed-Bessudo C, Tuross N, Levy AA, Weiner S (2009) New methods to isolate organic materials from silicified phytoliths reveal fragmented glycoproteins but no DNA. Quatern Int 193: 11–19
Google Scholar: Author Only Title Only Author and Title

Farhat W, Venditti R, Quick A, Taha M, Mignard N, Becquart F, Ayoub A (2017) Hemicellulose extraction and characterization for applications in paper coatings and adhesives. Industrial Crops and Products 107: 370–377
Google Scholar: Author Only Title Only Author and Title

Fleck AT, Nye T, Repenning C, Stahl F, Zahn M, Schenk MK (2011) Silicon enhances suberization and lignification in roots of rice (Oryza sativa). J Exp Bot 62: 2001–2011
Google Scholar: Author Only Title Only Author and Title

Fry SC, Willis SC, Paterson AEJ (2000) Intraprotoplasmic and wall-localised formation of arabinoxylan-bound diferulates and larger ferulate coupling-products in maize cell-suspension cultures. Planta 211: 679–692
Google Scholar: Author Only Title Only Author and Title

Harrison CC (1996) Evidence for intramineral macromolecules containing protein from plant silicas. Phytochemistry 41: 37–42
Google Scholar: Author Only Title Only Author and Title

Hatfield RD, Rancour DM, Marita JM (2017) Grass cell walls: A story of cross-linking. Front Plant Sci 7: 2056
Google Scholar: Author Only Title Only Author and Title

Hodson MJ (2016) The development of phytoliths in plants and its influence on their chemistry and isotopic composition. Implications for palaeoecology and archaeology. Journal of Archaeological Science 68: 62–69
Google Scholar: Author Only Title Only Author and Title

Hoffmann N, Benske A, Betz H, Schuetz M, Samuels AL (2020) Laccases and Peroxidases Co-Localize in Lignified Secondary Cell Walls throughout Stem Development. Plant Physiology 184: 806–822
Google Scholar: Author Only Title Only Author and Title

Kreszies T, Kreszies V, Ly F, Thangamani PD, Shellakkutti N, Schreiber L (2020) Suberized transport barriers in plant roots: the effect of silicon. J Exp Bot. doi: 10.1093/jxb/eraa203
Google Scholar: Author Only Title Only Author and Title

Kumar S, Adiram-Filiba N, Blum S, Sanchez-Lopez JA, Tzfadia O, Omid A, Volpin H, Heifetz Y, Goobes G, Elbaum R (2020) Siliplant1 protein precipitates silica in sorghum silica cells. Journal of Experimental Botany eraa258
Google Scholar: Author Only Title Only Author and Title

Kumar S, Elbaum R (2018) Interplay between silica deposition and viability during the life span of sorghum silica cells. New Phytol 217: 1137–1145
Google Scholar: Author Only Title Only Author and Title

Kumar S, Milstein Y, Brami Y, Elbaum M, Elbaum R (2017) Mechanism of silica deposition in sorghum silica cells. New Phytol 213: 791–798
Google Scholar: Author Only Title Only Author and Title

Lawton JR (1980) Observations on the structure of epidermal cells, particularly the cork and silica cells, from the flowering stem internode of Lolium temulentum L. (Gramineae). Bot J Linn Soc 80: 161–177
Google Scholar: Author Only Title Only Author and Title

Lee Y, Rubio MC, Alassimone J, Geldner N (2013) A mechanism for localized lignin deposition in the endodermis. Cell 153: 402–412
Google Scholar: Author Only Title Only Author and Title

Liang Y, Sun W, Zhu YG, Christie P (2007) Mechanisms of silicon-mediated alleviation of abiotic stresses in higher plants: a review. Environ Pollut 147: 422–428
Google Scholar: Author Only Title Only Author and Title

Lukačová Z, Švubová R, Kohanová J, Lux A (2013) Silicon mitigates the Cd toxicity in maize in relation to cadmium translocation, cell distribution, antioxidant enzymes stimulation and enhanced endodermal apoplasmic barrier development. Plant Growth Regul 70: 89–103
Google Scholar: Author Only Title Only Author and Title

Lux A, Luxová M, Abe J, Tanimoto E, Hattori T, Inanaga S (2003) The dynamics of silicon deposition in the sorghum root endodermis. New Phytol 158: 437–441
Google Scholar: Author Only Title Only Author and Title

Meents MJ, Watanabe Y, Samuels AL (2018) The cell biology of secondary cell wall biosynthesis. Ann Bot 121: 1107–1125
Google Scholar: Author Only Title Only Author and Title

Mitani N, Ma JF, Iwashita T (2005) Identification of the silicon form in xylem sap of rice (Oryza sativa L.). Plant Cell Physiol 46: 279
Google Scholar: Author Only Title Only Author and Title

Mitani-Ueno N, Ma JF (2020) Linking transport system of silicon with its accumulation in different plant species. Soil Science and Plant Nutrition 0: 1–8
Google Scholar: Author Only Title Only Author and Title

Mittler R, Vanderauwera S, Gollery M, Van Breusegem F (2004) Reactive oxygen gene network of plants. Trends in Plant Science 9: 490–498
Google Scholar: Author Only Title Only Author and Title

Neill SJ, Desikan R, Clarke A, Hurst RD, Hancock JT (2002) Hydrogen peroxide and nitric oxide as signalling molecules in plants. J Exp Bot 53: 1237–1247
Google Scholar: Author Only Title Only Author and Title

Nuopponen M, Willför S, Jääskeläinen A-S, Vuorinen T (2004) A UV resonance Raman (UVRR) spectroscopic study on the extractable compounds in Scots pine (Pinus sylvestris) wood: Part II. Hydrophilic compounds. Spectrochimica Acta Part A: Molecular and Biomolecular Spectroscopy 60: 2963–2968
Google Scholar: Author Only Title Only Author and Title

Sakurai G, Satake A, Yamaji N, Mitani-Ueno N, Yokozawa M, Feugier FG, Ma JF (2015) In silico simulation modeling reveals the importance of the Casparian strip for efficient silicon uptake in rice roots. Plant Cell Physiol 56: 631–639
Google Scholar: Author Only Title Only Author and Title

Sangster AG, Parry DW (1976) Endodermal silicon deposits and their linear distribution in developing roots of Sorghum bicolor (L.) Moench. Ann Bot 40: 361–371
Google Scholar: Author Only Title Only Author and Title

Sattler SE, Saathoff AJ, Haas EJ, Palmer NA, Funnell-Harris DL, Sarath G, Pedersen JF (2009) A Nonsense Mutation in a Cinnamyl Alcohol Dehydrogenase Gene Is Responsible for the Sorghum brown midrib6 Phenotype. Plant Physiology 150: 584–595
Google Scholar: Author Only Title Only Author and Title

Schieber M, Chandel NS (2014) ROS function in redox signaling and oxidative stress. Current Biology 24: R453–R462
Google Scholar: Author Only Title Only Author and Title

Schneider CA, Rasband WS, Eliceiri KW (2012) NIH Image to ImageJ: 25 years of image analysis. Nature methods 9: 671
Google Scholar: Author Only Title Only Author and Title

Schuetz M, Benske A, Smith RA, Watanabe Y, Tobimatsu Y, Ralph J, Demura T, Ellis B, Samuels AL (2014) Laccases direct lignification in the discrete secondary cell wall domains of protoxylem. Plant Physiology 166: 798–807
Google Scholar: Author Only Title Only Author and Title

Smith FA, Anderson KB (2001) Characterization of organic compounds in phytoliths: improving the resolving power of phytolith 13C as a tool for paleoecological reconstruction of C3 and C4 grasses. Phytoliths: Applications in Earth Sciences and Human History Lisse: AA Balkema Publishers p 317–27
Google Scholar: Author Only Title Only Author and Title

Soukup M, Martinka M, Bosnić D, Čaplovičová M, Elbaum R, Lux A (2017) Formation of silica aggregates in sorghum root endodermis is predetermined by cell wall architecture and development. Ann Bot 120: 739–753
Google Scholar: Author Only Title Only Author and Title

Soukup M, Martinka M, Cigáň M, Ravaszová F, Lux A (2014) New method for visualization of silica phytoliths in Sorghum bicolor roots by fluorescence microscopy revealed silicate concentration-dependent phytolith formation. Planta 240: 1365–1372
Google Scholar: Author Only Title Only Author and Title

Soukup M, Rodriguez Zancajo VM, Kneipp J, Elbaum R (2019) Formation of root silica aggregates in sorghum is an active process of the endodermis. J Exp Bot erz387
Google Scholar: Author Only Title Only Author and Title

Stewart D, Yahiaoui N, McDougall GJ, Myton K, Marque C, Boudet AM, Haigh J (1997) Fourier-transform infrared and Raman spectroscopic evidence for the incorporation of cinnamaldehydes into the lignin of transgenic tobacco (Nicotiana tabacum L.) plants with reduced expression of cinnamyl alcohol dehydrogenase. Planta 201: 311–318
Google Scholar: Author Only Title Only Author and Title

Taylor LS, Zografi G (1997) Spectroscopic Characterization of Interactions Between PVP and Indomethacin in Amorphous Molecular Dispersions. Pharm Res 14: 1691–1698
Google Scholar: Author Only Title Only Author and Title

Tsukagoshi H, Busch W, Benfey PN (2010) Transcriptional Regulation of ROS Controls Transition from Proliferation to Differentiation in the Root. Cell 143: 606–616
Google Scholar: Author Only Title Only Author and Title

Van Bockhaven J, Vleesschauwer DD, Höfte M (2013) Towards establishing broad-spectrum disease resistance in plants: silicon leads the way. J Exp Bot 64: 1281–1293
Google Scholar: Author Only Title Only Author and Title

Wang Y, Chantreau M, Sibout R, Hawkins S (2013) Plant cell wall lignification and monolignol metabolism. Front Plant Sci 4: 220
Google Scholar: Author Only Title Only Author and Title

Yahiaoui N, Marque C, Myton KE, Negrel J, Boudet AM (1997) Impact of different levels of cinnamyl alcohol dehydrogenase down-regulation on lignins of transgenic tobacco plants. Planta 204: 8–15
Google Scholar: Author Only Title Only Author and Title

Yang H, Yan R, Chen H, Lee DH, Zheng C (2007) Characteristics of hemicellulose, cellulose and lignin pyrolysis. Fuel 86: 1781–1788
Google Scholar: Author Only Title Only Author and Title

Yoshida S (1981) Fundamentals of rice crop science. International Rice Research Institute (IRRI), Los Baños, Laguna, Philippines
Google Scholar: Author Only Title Only Author and Title

Zancajo VMR, Diehn S, Filiba N, Goobes G, Kneipp J, Elbaum R (2019) Spectroscopic discrimination of sorghum silica phytoliths. Front Plant Sci 10: 1571
Google Scholar: Author Only Title Only Author and Title

Zexer N, Elbaum R (2020) Unique lignin modifications pattern the nucleation of silica in sorghum endodermis. J Exp Bot 71: 6818–6829
Google Scholar: Author Only Title Only Author and Title